applied optics

Comparative study on passive and active projector nonlinear gamma calibration

SONG ZHANG

School of Mechanical Engineering, Purdue University, West Lafayette, Indiana 47907, USA (szhang15@purdue.edu)

Received 14 January 2015; revised 29 March 2015; accepted 29 March 2015; posted 30 March 2015 (Doc. ID 232540); published 21 April 2015

This paper compares the active and passive projector nonlinear gamma compensation methods for phase error reduction. The *active method* modifies fringe patterns before their projection to ensure sinusoidality; the *passive method*, in contrast, compensates for the phase error after capturing those distorted sinusoidal fringe patterns. Our study finds that the active method tends to provide more consistent high-quality fringe patterns regardless of the amount of projectors defocusing; yet the effectiveness of the passive method is diminished if the measurement condition deviates from the calibration condition. Experimental results will be presented to demonstrate the differences between these two nonlinear gamma compensation methods.

OCIS codes: (120.0120) Instrumentation, measurement, and metrology; (120.2650) Fringe analysis; (100.5070) Phase retrieval.

http://dx.doi.org/10.1364/AO.54.003834

1. INTRODUCTION

High-speed and high-accuracy 3D optical metrology techniques have been successfully applied to numerous areas including medicine, computer science, and manufacturing industry. Over the past few decades, many methods [1] have been developed to recover 3D surface geometry using different principles [2,3]. These methods include time of flight, laser triangulation, shape from focus and defocus, stereo vision, structured light, and digital fringe projection (DFP). Among these methods, DFP techniques have been increasingly used because of the merits of high speed and high accuracy [4].

It is well known that the success of accurate 3D shape measurement using a DFP method heavily relies on the recovered phase quality if a single projector and a single camera are used. This is because such systems recover 3D geometry directly from phase, indicating that any phase noise or distortion will be reflected on final measurements. Among various major error sources, the nonlinear response to input images is one critical error source to handle if one uses a commercially available digital video projector: this error source often refers to the nonlinear gamma effect. Using more fringe patterns [5–7] could reduce certain types of harmonics, and thus improve measurement quality. However, using more patterns will sacrifice measurement speeds, which is not desirable for high-speed applications. The binary defocusing technology [8,9] could also diminish the nonlinear influence, but it yields a lower signal-to-noise ratio (SNR).

The majority of state-of-the-art research focuses on calibrating the nonlinear response of a DFP system and then compensating for the associated error. Though numerous nonlinear gamma calibration and error compensation methods have been developed, they can be broadly classified into two categories: actively modifying the fringe patterns before their projection [10,11] or passively compensating phase error after the fringe patterns are captured [12–22]. The majority of research focused on estimating nonlinear gamma coefficients through different algorithms from the captured fringe patterns, and some by directly calibrating the gamma of the projector. Both active and passive methods have been demonstrated successful to substantially reduce the phase error caused by the projector's nonlinear gamma. However, to our knowledge, there is no study to directly compare the effectiveness of these two types of error compensation methods (i.e., active and passive methods) when the system is not operating under its calibrated settings, i.e., when the projector has a different amount of defocusing, albeit Ref. [11] mentioned the projector's defocusing effect.

This paper presents a study examining the influence of projector defocusing on the effectiveness of these two different error compensation methods. Our study finds that an active method tends to provide more consistent high-quality fringe patterns regardless of the amount of defocusing, yet the effectiveness of a passive method is sensitive to the measurement conditions, although the passive method could provide equally good quality phase under its optimal calibration condition. This research finding coincides with our prior study on the binary defocusing technique in which the phase error varies with different amounts of defocusing [16], and thus compensating the phase error passively in the phase domain is more difficult than actively modifying the fringe patterns before their projection.

Section 2 discusses the phase-shifting algorithm we used to evaluate phase quality, and explains two different phase error compensation methods. Section 3 presents some experimental results, and Section 4 summarizes this paper.

2. PRINCIPLE

A. Three-Step Phase-Shifting Algorithm

Phase-shifting algorithms have been extensively employed in optical metrology due to their speed, accuracy, and robustness to noise [7]. Even though numerous phase-shifting algorithms have been developed, a simple three-step phase-shifting algorithm is usually preferable for high-speed applications. This is because a three-step algorithm uses the minimum number of patterns required to solve for the phase value pixel by pixel without using global [23] or local [24] neighboring pixel information. A three-step phase-shifting algorithm with a phase shift of $2\pi/3$ can be realized by capturing three fringe images with equal phase shifts that can be mathematically described as

$$I_1(x,y) = I'(x,y) + I''(x,y)\cos[\phi - 2\pi/3], \tag{1}$$

$$I_2(x,y) = I'(x,y) + I''(x,y)\cos[\phi], \tag{2}$$

$$I_3(x,y) = I'(x,y) + I''(x,y)\cos[\phi + 2\pi/3]. \tag{3}$$

Here $I'(x,y)$ is the average intensity, $I''(x,y)$ is the intensity modulation, and $\phi(x,y)$ is the phase to be solved for. Simultaneously solving Eqs. (1)–(3) gives the phase

$$\phi(x,y) = \tan^{-1}\frac{\sqrt{3}(I_1 - I_3)}{2I_2 - I_1 - I_3}. \tag{4}$$

Since an arctangent function only provides phase values ranging from $-\pi$ to π, the phase obtained here is often called a wrapped phase with a modulus of 2π, and a spatial or temporal phase-unwrapping algorithm is required to resolve the 2π ambiguity [25]. Once the system is calibrated, (x, y, z) coordinates can be reconstructed from the unwrapped continuous phase [26].

B. Nonlinear Gamma Model

In the literature, a projector's nonlinear gamma was extensively modeled to be a simple function in the form of

$$I_o = a(I_i)^\gamma + b, \tag{5}$$

where I_o is the output grayscale value for a given input value I_i, a and b are constants, and γ is the unknown constant to be calibrated. For such a model, estimating the nonlinear effect of the digital video projector essentially is to determine γ. The calibration of constants a and b will not affect the phase quality since they can be optimized by properly adjusting the camera settings. Estimating γ can be realized through harmonic analysis, least squares, statistical methods, or directly analyzing the phase error by comparing with the ideal phase map.

Over the past few decades, we have used more than 10 different models as old as Kodak DP900, to Optoma EP739, and to the latest models such as LG PB63U and Dell M115HD; the nonlinear gamma varies from one model to another, and even from one projector to another with the same model. The gamma curve of more recent models tends to be smoother than for older models with LED projectors being remarkably smooth. Our research found that the nonlinear gamma of the majority of projectors we have used in our laboratory does not precisely follow such a simple model if the full range of grayscale values is used. Instead, we found that modeling the projectors' nonlinear gamma with a seventh-order polynomial function is sufficient and reliable for all the projectors [10]. That is, the gamma function is described as

$$I_o = c_0 + c_1 I_i + \cdots + c_6(I_i)^6 + c_7(I_i)^7, \tag{6}$$

where $c_0, c_1, \ldots, c_6, c_7$ are those constants to be calibrated.

C. Active Error Compensation Method

Active error compensation is more complex because the calibration condition could be different from case to case, and the modeling should be generic to any sort of captured calibration data. In this paper, we use the slightly improved method originally presented in Ref. [10].

Figure 1(a) illustrates the nonlinear gamma curve and the designed linear response curve. The nonlinear curve can be obtained by projecting a sequence of uniform grayscale images with different grayscale values, I_{ci}, and capturing them by a camera. By analyzing a small area of the camera image, the average value is treated as the output data, I_{c0}. It should be noted that the starting and ending points of the curve are not, respectively, always 0 and 255 to make the approach generic.

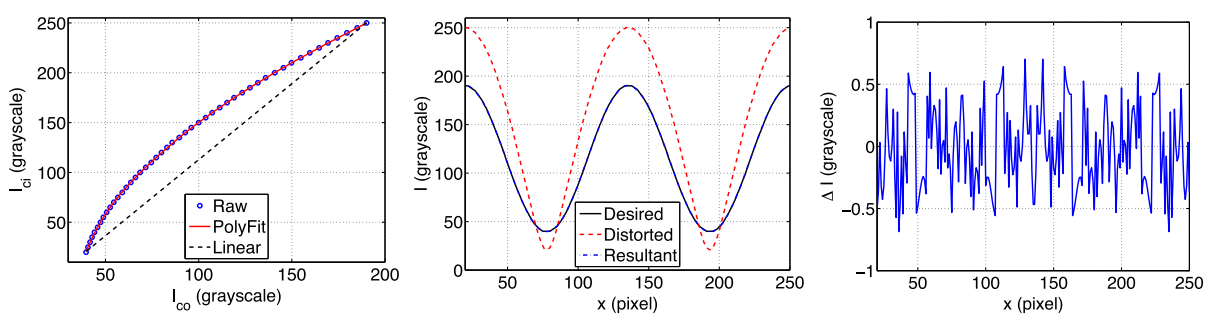

Fig. 1. Example of using an active error compensation method to model nonlinear gamma. (a) Nonlinear gamma curve, fitted polynomial curve, and the desired linear curve. (b) Desired ideal sinusoidal wave, actively distorted wave, and the resultant sinusoidal wave with nonlinear gamma correction. (c) Difference between ideal sinusoidal wave and the resultant sinusoidal wave with nonlinear gamma correction.

Since the active calibration method requires modifying the computer generated fringe patterns and predistorting the fringe patterns before their projection, the calibration is actually to determine the inverse function of the projector's nonlinear gamma. Instead of obtaining a polynomial function using Eq. (6), we fit the inverse function with the output as the x axis. That is, the polynomial function here is actually

$$I_{ci} = a_0 + a_1(I_{co}^s) + \cdots + a_6(I_{co}^s)^6 + a_7(I_{co}^s)^7. \quad (7)$$

Here a_k are constants that can be determined by using a set of calibration data.

The objective here is to determine the desired grayscale value, I_d, to be projected for a given value, I_g, such that the projected image will be ideally sinusoidal. Mathematically, I_d can be determined using

$$I_d = a_0 + a_1(I_g^s) + \cdots + a_6(I_g^s)^6 + a_7(I_g^s)^7, \quad (8)$$

where

$$I_g^s = \kappa \times (I_g - I_o^{\min}) + I_o^{\min} \quad (9)$$

is the modified given input value to consider the fact that the calibrated data range may not be 0 to 255. Here,

$$\kappa = \frac{I_o^{\max} - I_o^{\min}}{I_{ci}^{\max} - I_{ci}^{\min}} \quad (10)$$

is the slope of the desired linear response with

$$I_o^{\min} = c_0 + c_1[\min(I_{ci})] + \cdots + c_6[\min(I_{ci})]^6 + c_7[\min(I_{ci})]^7, \quad (11)$$

$$I_o^{\max} = c_0 + c_1[\max(I_{ci})] + \cdots + c_6[\max(I_{ci})]^6 + c_7[\max(I_{ci})]^7. \quad (12)$$

Here min() and max() are the minimum and maximum functions, and c_k are from the polynomial function determined using Eq. (6). Instead of directly using the captured data (i.e., $I_{co}^{\min}$ and $I_{co}^{\max}$) as in Ref. [10], we calculated $I_o^{\min}$ and $I_o^{\max}$ using the fitted polynomial function to reduce the noise influence of the raw captured data on both ends.

Figure 1(b) depicts the projected sinusoidal wave, the ideal sinusoidal wave, and the corrected sinusoidal wave using the nonlinear gamma curve shown in Fig. 1(a). Once the distorted curve is modulated by the nonlinear gamma function fitted by Eq. (6), the output curve should be identical to the ideal sinusoidal wave. This simulation clearly shows that the projected curve, as expected, perfectly overlaps with the ideal sinusoidal wave and the difference is purely random, as illustrated in Fig. 1(c).

D. Passive Error Compensation Method

The passive error compensation method, in contrast, does not modify the projector's input fringe patterns, but rather determines the phase error from the calibrated gamma curve, and then compensates for the phase error in phase domain. It is straightforward to determine the phase error for each phase value using the following steps if the projector's nonlinear gamma curve is obtained:

- *Step 1:* Compute the ideal phase-shifted fringe patterns. In our case, we use a three-step phase-shifting algorithm as described in Eqs. (1)–(3). Only one period of fringe patterns and one cross section of the sinusoidal patterns are necessary for further analysis.
- *Step 2:* Apply the nonlinear fitted gamma equation as described in Eq. (6) to generate the distorted curve with gamma effect. Figure 2(a) shows one of the distorted waves by the nonlinear gamma shown in Fig. 1(a).
- *Step 3:* Compute the ideal phase, Φ^i, using three ideal sinusoidal waves.
- *Step 4:* Compute the distorted phase, Φ^d, using three distorted waves. Figure 2(b) shows the ideal phase and the distorted phase. It clearly shows that significant phase error is introduced by the nonlinear gamma.
- *Step 5:* Compute phase error by simply taking the difference between the ideal phase and the distorted phase, i.e., $\Delta\Phi(\Phi^d) = \Phi^d - \Phi^i$.

Once the phase error for each distorted phase value is determined, it can be used to compensate for phase error introduced by the nonlinear gamma effect. Since the error compensation is pixel by pixel for each measurement, the computational cost could be substantial. To reduce computational cost, Zhang and Huang proposed to use a look-up table (LUT) (e.g., 256 elements) [13]. Generating the LUT is the process of evenly sampling the error curve and storing the phase error values for each phase value. It is important to note the x axis in Fig. 2(c) is the *distorted* phase map Φ^d that is the sampling space we should use. Compensation of the phase error can be done by locating the nearest LUT element or involving

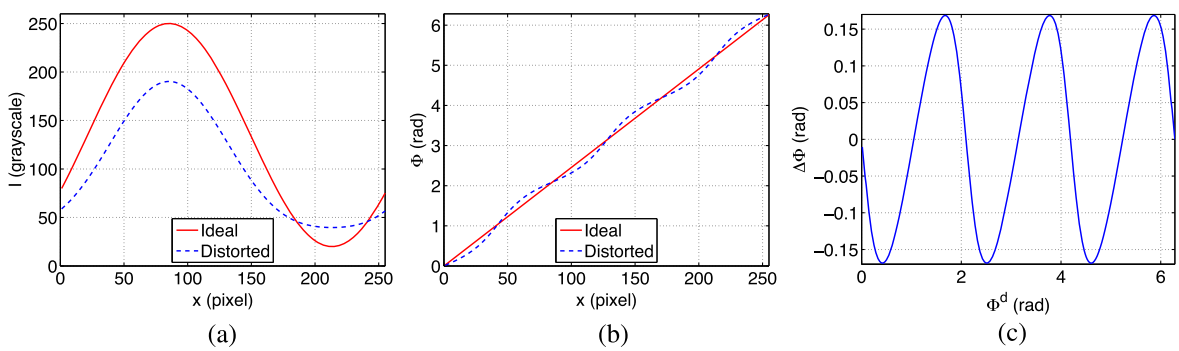

Fig. 2. Example of determining phase error based on calibrated gamma curve. (a) Simulated ideal sinusoidal wave and the distorted wave by gamma effect. (b) Ideal phase Φ^i versus distorted phase Φ^d. (c) Phase error induced by nonlinear gamma.

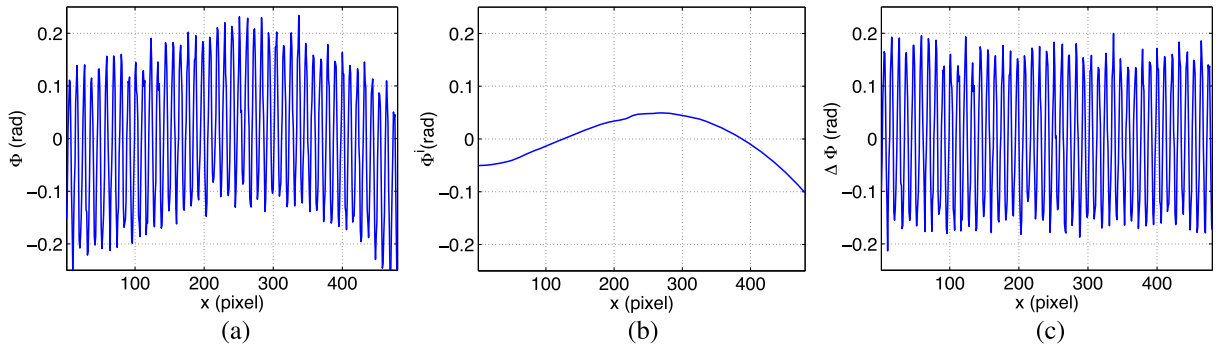

Fig. 3. Phase measurement error of the hardware system without nonlinear gamma correction. (a) Cross section of the unwrapped phase map after removing gross slope. (b) Cross section of the ideal unwrapped phase map after removing gross slope. (c) Cross section of the phase error map without gamma correction (rms of 0.116 mm).

linear or nonlinear interpolation, and then adding $\Delta\Phi$ to the phase value of that particular point.

3. EXPERIMENTS

A. Hardware System Setup

A hardware system was used to evaluate the performance of these nonlinear gamma calibration methods. The system includes a digital-light-processing (DLP) projector (Samsung SP-P310MEMX) and a charge-coupled-device (CCD) camera (Jai Pulnix TM-6740CL). The camera is attached with a 16 mm focal length mega-pixel lens (Computar M1614-MP) with F/1.4 to 16C. The projector resolution and the camera resolution are 800×600 and 640×480, respectively. A uniform flat white board was used as an imaging target for error analysis. It should be noted that the flat board and the camera remain untouched for all the experiments.

The projector's nonlinear gamma curve was obtained by projecting a sequence of unique grayscale images (from 20 to 250) with a grayscale value increment of 5. The camera captures the sequence of images, and the grayscale value for each input image is determined by averring a small area (5×5 pixels) in the center of each captured image. Figure 1(a) actually shows the gamma curve of this particular projector.

When ideal sinusoidal patterns generated by a computer are directly sent to the projector, the resultant phase error is significant due to the projector's nonlinear gamma effect. To demonstrate this, we projected ideal sinusoidal fringe patterns onto the white board and captured three phase-shifted fringe images while the projector was in focus. The phase was calculated by applying a phase-wrapping and a temporal phase-unwrapping algorithm. Figure 3(a) shows one cross section of the unwrapped phase map. To better visualize the phase error, the gross slope of the phase line was removed.

To quantify phase error, we took the difference between this phase map and the ideal phase map Φ^i. The ideal phase map was obtained by using the squared binary phase-shifting method [9] with a fringe period of 18 pixels for the projected fringe patterns. The squared binary phase-shifting method can generate high-quality phase without the influence of the nonlinear gamma effect of the projector if a larger number of patterns is used (nine in our case) using the least-square algorithm [27]. Again, a temporal phase-unwrapping algorithm was used to obtain raw phase that was further smoothed by a large Gaussian filter (e.g., 31×31 pixels) to structural error caused by our system. Figure 3(b) shows the ideal phase after removing its gross slope, which is very smooth, confirming that no obvious systematic structural error was introduced by the ideal phase map, Φ^i. The phase error map was calculated by taking the difference between the captured phase and the ideal phase (i.e., $\Delta\Phi = \Phi - \Phi^i$). Figure 3(c) shows one cross section of

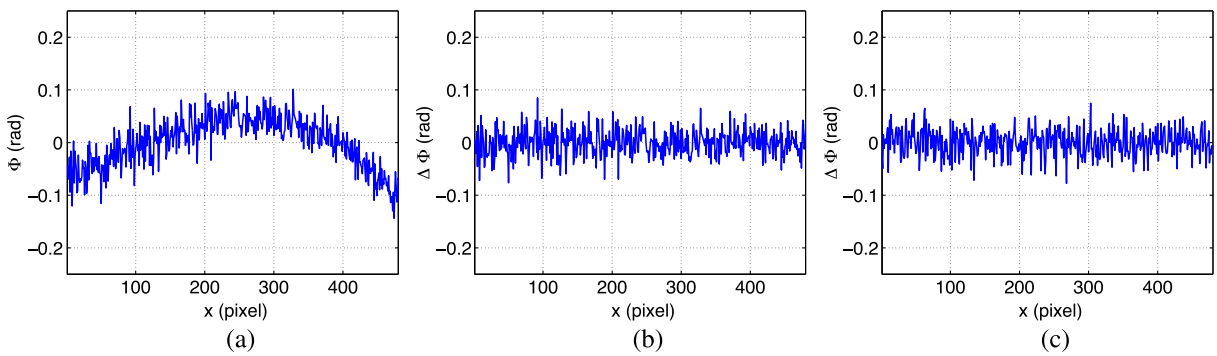

Fig. 4. Passive and active phase error compensation result. (a) Cross section of the unwrapped phase map with active error compensation after removing gross slope. (b) Cross section of the phase error map after active error compensation (rms 0.025 rad). (c) Cross section of the phase error map with passive error compensation (rms 0.025 rad).

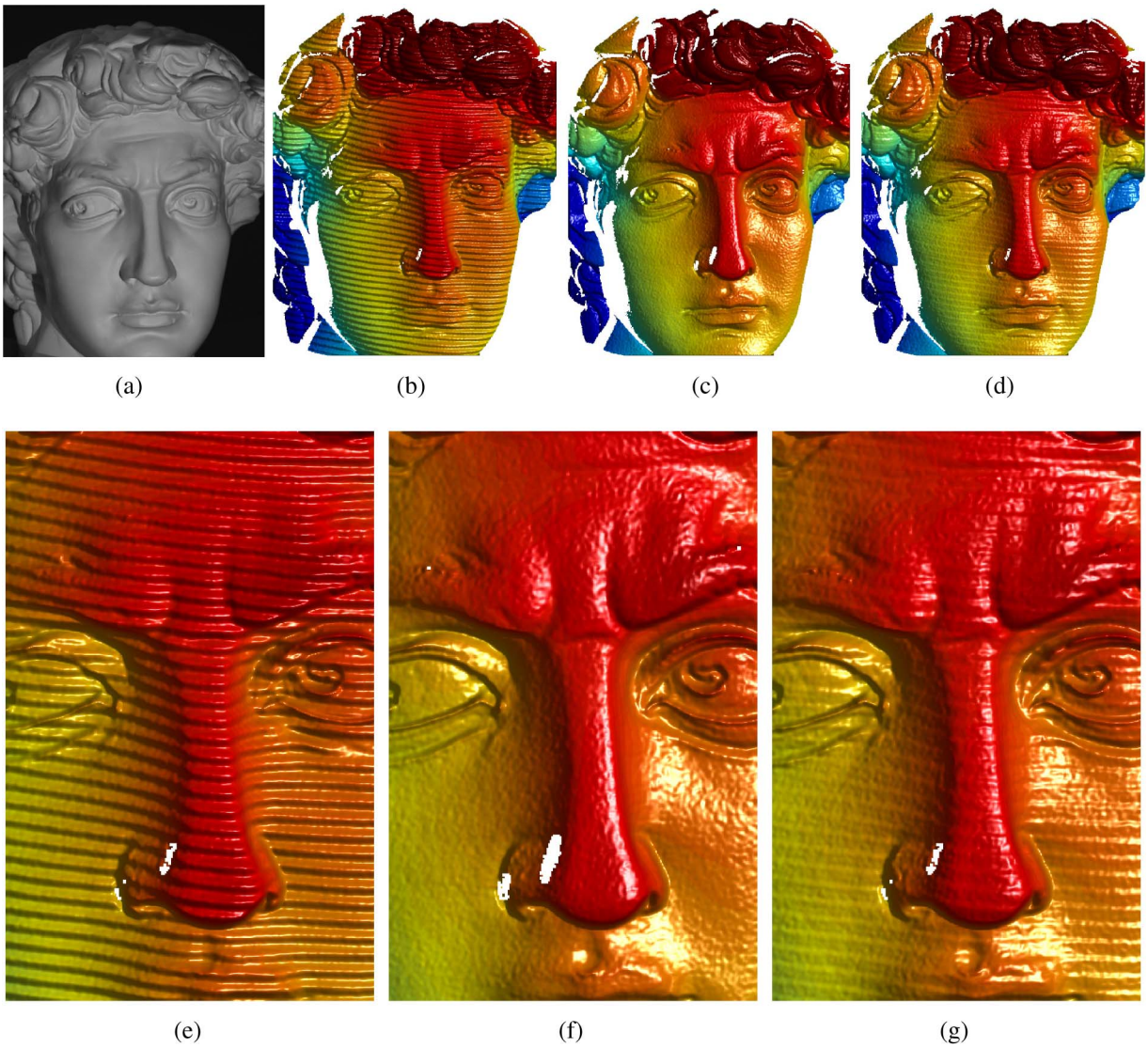

Fig. 5. Measurement results of statue. (a) Photograph of the statue. (b) 3D result before gamma compensation. (c) 3D result with active error compensation method. (d) 3D result with passive error compensation method. (e) Zoom-in view of (b). (f) Zoom-in view of (c). (g) Zoom-in view of (d).

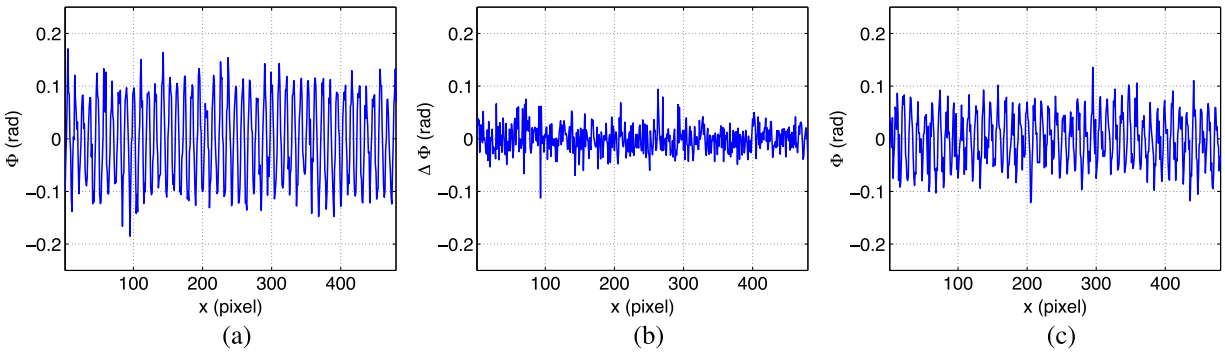

Fig. 6. Phase error compensation results when projector is out of focus. (a) Cross section of phase error map without any error compensation (rms 0.080 rad). (b) Cross section of the phase error map with active error compensation method (rms 0.026 rad). (c) Cross section of the phase error map with passive error compensation method (rms 0.049 rad).

the phase error map. If nonlinear gamma is not considered, the phase error is very large with a root-mean-square (rms) value of 0.116 rad.

B. Experimental Results for In-Focus Projector

Using the calibrated gamma curve, we predistorted the projected fringe patterns using the method discussed in Subsection 2.C and projected those distorted patterns onto the white board. Figure 4(a) shows one cross section of the captured phase after removing its gross slope. Comparing with the result shown in Fig. 3(a), the phase does not have any obvious structural error. Figure 4(b) shows one cross section of the phase error with a phase rms error of 0.025 rad, proving the effectiveness of active error compensation.

We then captured three phase-shifted fringe patterns using exactly the same settings, except the projector's input fringe patterns are ideal sinusoidal (the same images as those used in Fig. 3). Figure 4(c) shows the phase error after error compensation using the 512-element LUT discussed in Subsection 2.D. This experiment shows that passive error compensation can also effectively reduce the phase rms error from 0.116 to 0.025 rad. Compared with the active method, the passive method performs equally well.

We also measured a statue to visually compare the differences of these error compensation methods. Figure 5 shows the results. Unlike the previous flat board, the statue actually has certain depth variations. As shown in Figs. 5(b) and 5(e), before error compensation, the structural error is very

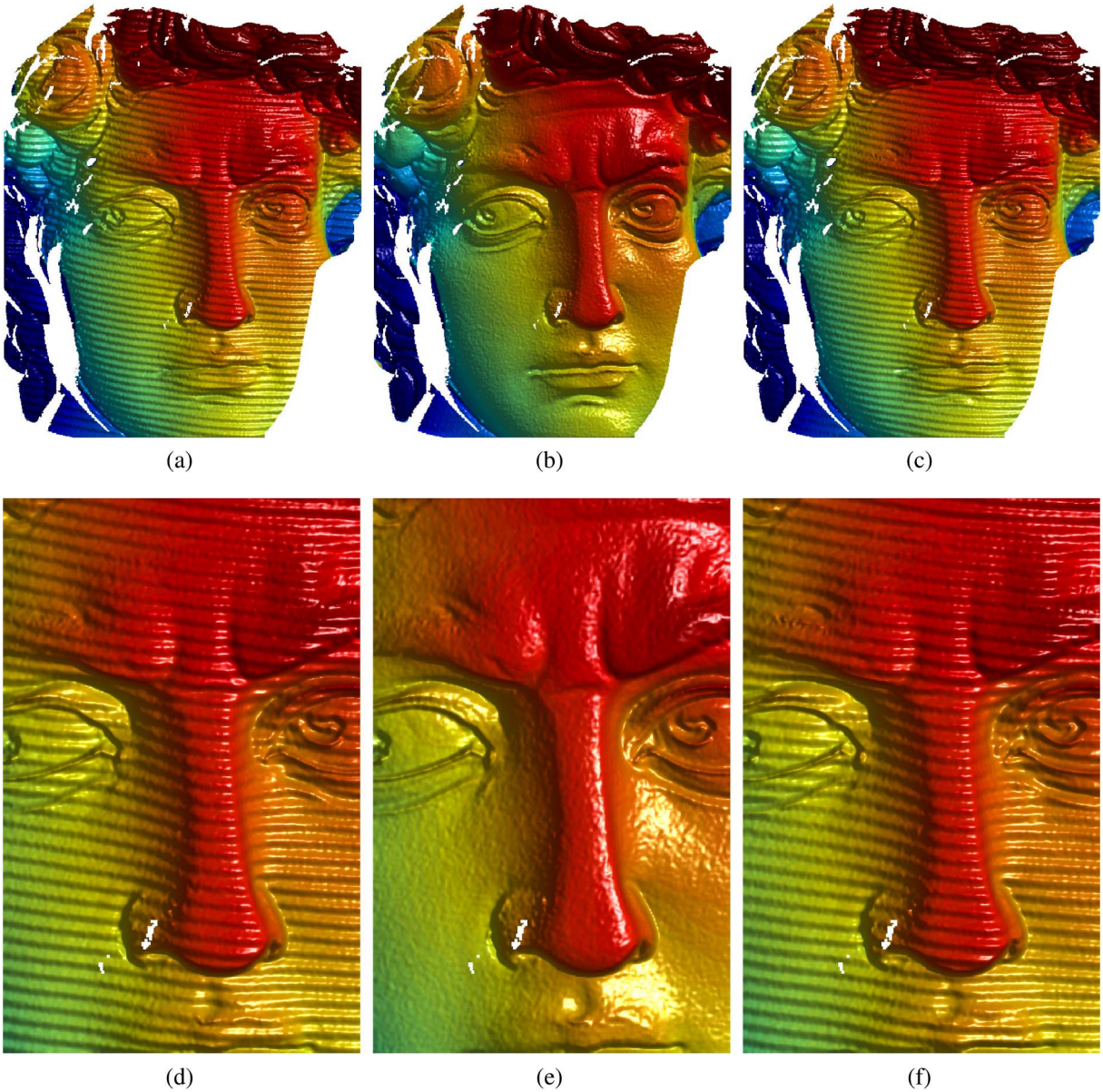

Fig. 7. Measurement results of statue when the projector is out of focus. (a) 3D result before gamma compensation. (b) 3D result with active error compensation method. (c) 3D result with passive error compensation method. (d) Zoom-in view of (a). (e) Zoom-in view of (b). (f) Zoom-in view of (c).

obvious. The active error compensation method provides very high-quality 3D shape measurement without obvious error caused by the nonlinear gamma effect, as shown in Figs. 5(c) and 5(f). Figures 5(d) and 5(g) show the results after applying the passive error compensation method. Even though these results are fairly good, the quality is not as high as that using the active method. We believe this was caused by the fact that the object surface does not always stay in the same amount of defocusing, even when the projector is in focus. These experiments visually demonstrated that the active method outperforms the passive method even when the measurement is close to the calibration condition. It should be noted that all the 3D rendered results were smoothed with a 3×3 Gaussian filter to suppress the most significant random noise.

C. Experimental Results for Defocused Projector

In practical measurement conditions, the object may be placed further away from the gamma calibration plane, meaning the projector may not be perfectly at the same amount of defocusing. To emulate this effect, we changed the focal plane of the projector, making the projected image blurred on the flat board. We then repeated the same analyses. Figure 6 shows the results. Comparing the results shown in Fig. 6(a) and Fig. 3(c), we can see that the phase error induced by nonlinear gamma is reduced because of defocusing (rms 0.116 versus rms 0.080). One may notice that the active method still performs well [refer to Fig. 6(b)], but the passive method has significant residual structural error [refer to Fig. 6(c)]. This is because the defocusing effect actually changes the inherent structures of the fringe patterns if they are not ideally sinusoidal, but does not alter sinusoidal pattern structures for ideal sinusoidal patterns. One may notice that the overall phase error for the active method is also slightly increased because of the lower fringe contrast. This coincides with our prior study [16] that demonstrated that the phase error is indeed different for different amounts of defocusing [although that study shows a different type of nonsinusoidal structured patterns (i.e., squared binary patterns)].

Again, the statue was measured when the projector was defocused. Figure 7 shows the results. Figures 7(b) and 7(e) indicate that the active error compensation method still generated good-quality data. However, the passive error compensation method fails to produce high-quality results, as shown in Figs. 7(c) and 7(f). These experimental results demonstrated that the active method works much better than the passive method when a different amount of defocusing is used for nonlinear gamma calibration and real measurement. Additionally, comparing Figs. 7(a) and 7(d) with Figs. 5(b) and 5(e), one may also notice that, without applying any error compensation, the measurement results are much better when the projector is out of focus than when the projector is in focus. This is because projector defocusing can naturally suppress the nonlinearity of the projector's gamma effect.

Lastly, we performed experiments when the projector was at different amounts of defocusing. Figure 8 shows the phase rms error when the projector was at fixed different defocusing levels (i.e., from nearly focused, Level 1, to substantially defocused, Level 6). This figure shows that increased defocusing degree (1) diminishes the nonlinear gamma effect of the projector without any compensation; (2) does not obviously affect the active nonlinear gamma calibration method, although the phase error increases slightly when the projector is defocused too much; and (3) adversely changes the effectiveness of the passive nonlinear gamma calibration method. It should be noted that this set of data was captured using a newer model projector, LG PB63U, to show the variations of hardware selection.

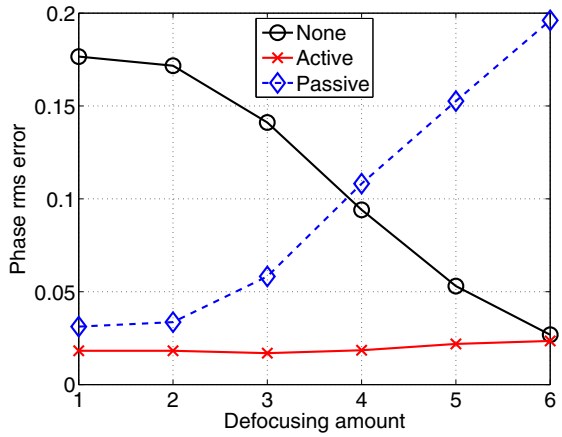

Fig. 8. Comparison of different error compensation methods with different amounts of projector defocusing.

We would like to point out the fact that not all system nonlinear gamma curves can be directly calibrated as they are to digital video projectors, or the projected patterns can be predistorted. Therefore, for many practical systems, passive error compensation methods have to be adopted. Yet, this paper provides the insight that for such systems, if the projection system has a different amount of defocusing, a simple error calibration may not be sufficient.

4. CONCLUSIONS

This paper compares the study of the passive and active projectors' nonlinear gamma calibration methods. It reveals that if the measurement conditions are exactly the same as the calibration conditions (e.g., the projector has the same degree of defocusing, and the object is on the same plane as the calibration board), both active and passive methods can perform equally well. However, when the object is at different locations or the projector's focus is changed, the effectiveness of the active method does not change noticeably, but the passive method fails to effectively reduce the phase error caused by the projector's nonlinear gamma. Therefore, it appears that an active method is preferable if such a method can be adopted, and if only a passive method can be used, caution should be given to the calibration conditions and the measurement conditions.

National Science Foundation (NSF) Directorate for Engineering (ENG) (CMMI-1300376). The views expressed in this paper are those of the authors and not necessarily those of the NSF.

When the majority of this work was completed, Professor Song Zhang was affiliated with Iowa State University, Ames, Iowa, USA.

REFERENCES

1. S. Zhang, ed., *Handbook of 3D Machine Vision: Optical Metrology and Imaging*, 1st ed. (CRC Press, 2013).
2. J. Geng, "Structured-light 3D surface imaging: a tutorial," Adv. Opt. Photon. **3**, 128–160 (2011).
3. S. Gorthi and P. Rastogi, "Fringe projection techniques: whither we are?" Opt. Lasers Eng. **48**, 133–140 (2010).
4. S. Zhang, "Recent progresses on real-time 3-D shape measurement using digital fringe projection techniques," Opt. Lasers Eng. **48**, 149–158 (2010).
5. P. S. Huang, Q. J. Hu, and F.-P. Chiang, "Double three-step phase-shifting algorithm," Appl. Opt. **41**, 4503–4509 (2002).
6. S. Zhang, "High-resolution three-dimensional profilometry with binary phase-shifting methods," Appl. Opt. **50**, 1753–1757 (2011).
7. H. Schreiber and J. H. Bruning, "Phase shifting interferometry," in *Optical Shop Testing*, 3rd ed. (Wiley, 2007), pp. 547–655.
8. X. Y. Su, W. S. Zhou, G. Von Bally, and D. Vukicevic, "Automated phase-measuring profilometry using defocused projection of a Ronchi grating," Opt. Commun. **94**, 561–573 (1992).
9. S. Lei and S. Zhang, "Flexible 3-D shape measurement using projector defocusing," Opt. Lett. **34**, 3080–3082 (2009).
10. P. S. Huang, C. Zhang, and F.-P. Chiang, "High-speed 3-D shape measurement based on digital fringe projection," Opt. Eng. **42**, 163–168 (2003).
11. X. Zhang, L. Zhu, Y. Li, and D. Tu, "Generic nonsinusoidal fringe model and gamma calibration in phase measuring profilometry," J. Opt. Soc. Am. A **29**, 1047–1058 (2012).
12. B. Pan, Q. Kemao, L. Huang, and A. Asundi, "Phase error analysis and compensation for nonsinusoidal waveforms in phase-shifting digital fringe projection profilometry," Opt. Lett. **34**, 2906–2914 (2009).
13. S. Zhang and P. S. Huang, "Phase error compensation for a three-dimensional shape measurement system based on the phase shifting method," Opt. Eng. **46**, 063601 (2007).
14. S. Zhang and S.-T. Yau, "Generic nonsinusoidal phase error correction for three-dimensional shape measurement using a digital video projector," Appl. Opt. **46**, 36–43 (2007).
15. H. Guo, H. He, and M. Chen, "Gamma correction for digital fringe projection profilometry," Appl. Opt. **43**, 2906–2914 (2004).
16. Y. Xu, L. Ekstrand, J. Dai, and S. Zhang, "Phase error compensation for three-dimensional shape measurement with projector defocusing," Appl. Opt. **50**, 2572–2581 (2011).
17. K. Liu, Y. Wang, D. L. Lau, Q. Hao, and L. G. Hassebrook, "Gamma model and its analysis for phase measuring profilometry," J. Opt. Soc. Am. A **27**, 553–562 (2010).
18. T. Hoang, B. Pan, B. Nguyen, and Z. Wang, "Generic gamma correction for accuracy enhancement in fringe projection profilometry," Opt. Lett. **35**, 1992–1994 (2010).
19. Z. Li and Y. Li, "Gamma-distorted fringe image modeling and accurate gamma correction for fast phase measuring profilometry," Opt. Lett. **36**, 154–156 (2011).
20. P. Zhou, X. Liu, Y. He, and T. Zhu, "Phase error analysis and compensation considering ambient light for phase measuring profilometry," Opt. Lasers Eng. **55**, 99–104 (2014).
21. S. Ma, R. Zhu, C. Quan, B. Li, C. J. Tay, and L. Chen, "Blind phase error suppression for color-encoded digital fringe projection profilometry," Opt. Commun. **285**, 1662–1668 (2012).
22. S. Ma, C. Quan, R. Zhu, L. Chen, B. Li, and C. J. Tay, "A fast and accurate gamma correction based on Fourier spectrum analysis for digital fringe projection profilometry," Opt. Lasers Eng. **285**, 533–538 (2012).
23. M. Takeda and K. Mutoh, "Fourier transform profilometry for the automatic measurement of 3-D object shape," Appl. Opt. **22**, 3977–3982 (1983).
24. Q. Kemao, "Windowed Fourier transform for fringe pattern analysis," Appl. Opt. **43**, 2695–2702 (2004).
25. D. C. Ghiglia and M. D. Pritt, *Two-Dimensional Phase Unwrapping: Theory, Algorithms, and Software* (Wiley, 1998).
26. S. Zhang and P. S. Huang, "Novel method for structured light system calibration," Opt. Eng. **45**, 083601 (2006).
27. L. Ekstrand and S. Zhang, "Three-dimensional profilometry with nearly focused binary phase-shifting algorithms," Opt. Lett. **36**, 4518–4520 (2011).